Journal of Hazardous Materials 485 (2025) 136895

Contents lists available at ScienceDirect

Journal of Hazardous Materials

journal homepage: www.elsevier.com/locate/jhazmat

A comprehensive atlas of multi-tissue metabolome and microbiome shifts: Exploring obesity and insulin resistance induced by perinatal bisphenol S exposure in high-fat diet-fed offspring

Shuyin Li [a,1], Longhua Gao [a,1], Haoyue Song [a], Jiayi Lin [a], Shen Zhang [c,d,*], Philippe Schmitt-Kopplin [b,**], Jun Zeng [a,b,e,***]

[a] College of Ocean Food and Biological Engineering, Jimei University, Xiamen 361021, China
[c] Clinical Research Center for Reproduction and Genetics in Hunan Province, Reproductive and Genetic Hospital of CITIC-XIANGYA, Changsha 410000, China
[d] NHC Key Laboratory of Human Stem Cell and Reproductive Engineering, School of Basic Medical Sciences, Central South University, Changsha 410075, China
[b] Research Unit Analytical BioGeoChemistry, Helmholtz Munich, Neuherberg 85764, Germany
[e] Xiamen Key Laboratory of Marine Functional Food, Xiamen 361021, China

HIGHLIGHTS

- Perinatal BPS exposure reduced glucose tolerance and insulin sensitivity in offspring.
- Male offspring showed greater multi-tissue metabolome and microbiome disturbances than females.
- Low-dose BPS exposure (0.05 mg/kg/d) induced atlas changes comparable to high-dose (5 mg/kg/d).
- Compensatory BAT thermogenesis and increased beneficial bacteria indicated a resistance mechanism to BPS exposure.
- Metabolic competition and imbalance between WAT and BAT contribute to offspring obesity and insulin resistance.

GRAPHICAL ABSTRACT

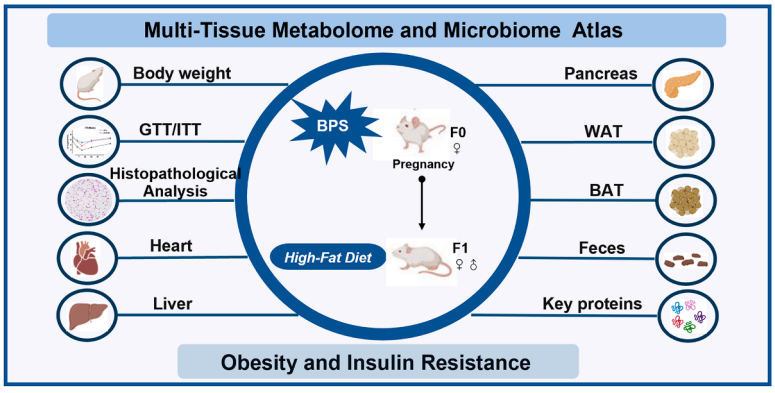

ARTICLE INFO

Keywords:
Bisphenol S
Metabolomics
Microbial community analysis

ABSTRACT

Bisphenol S (BPS) is widely used as a substitute for Bisphenol A (BPA). While perinatal BPS exposure is suspected to increase susceptibility to high-caloric diet-induced adipogenesis, how BPS affects offspring remains largely unknown. This study explored effects of prenatal BPS exposure on adiposity and insulin resistance in high-fat diet (HFD)-fed C57BL/6 offspring, revealing significant changes in body weight, glucose tolerance, insulin sensitivity,

* Corresponding author at: Clinical Research Center for Reproduction and Genetics in Hunan Province, Reproductive and Genetic Hospital of CITIC-XIANGYA, Changsha 410000, China.
** Corresponding author.
*** Corresponding author at: College of Ocean Food and Biological Engineering, Jimei University, Xiamen 361021, China
E-mail addresses: szhang231@126.com (S. Zhang), philippe.schmittkopplin@helmholtz-munich.de (P. Schmitt-Kopplin), junzeng@jmu.edu.cn, jun.zeng@helmholtz-munich.de (J. Zeng).
[1] Equal contribution.

https://doi.org/10.1016/j.jhazmat.2024.136895
Received 1 October 2024; Received in revised form 6 December 2024; Accepted 13 December 2024
Available online 15 December 2024

Insulin resistance
Perinatal exposure

and histopathology. Employing nontargeted metabolomics and 16S rRNA sequencing, we constructed a comprehensive atlas of metabolome and microbiome shifts across heart, liver, pancreas, white adipose tissue (WAT), brown adipose tissue (BAT), and feces. Male offspring showed greater metabolic and microbial disturbances. Low-dose BPS exposure (0.05 mg/kg/d) induced changes across entire atlas comparable to high-dose (5 mg/kg/d). BAT and WAT were key target tissues with the most significant metabolic disturbances. BPS disrupted fatty acid β-oxidation in WAT by reducing carnitine carriers, causing WAT fat accumulation. A resistance mechanism to BPS exposure was indicated by both mobilization of BAT compensatory thermogenesis, characterized by increased carnitines and UCP1 expression, and an increase in beneficial commensal bacteria. Their competition and imbalance contributed to obesity and insulin resistance in offspring, highlighting the potential for early interventions targeting key metabolites and microbiota.

1. Introduction

Obesity in young individuals is a growing public health concern, significantly elevating the risk of various metabolic disorders, including insulin resistance and type 2 diabetes. In addition to unhealthy high-caloric-density dietary patterns, there has been increasing attention on "obesogens"-environmental and food-derived pollutants [1,2]. These "obesogens" have been recognized as potential contributors to the rising risk of obesity [1,2].

Bisphenol S (BPS), a structural analog of Bisphenol A (BPA), has been widely adopted as a substitute in various products, including canned foodstuffs, food paperboard, epoxy resins, and thermal paper, following the restricted use of BPA [3]. Food is the primary route of BPS exposure. BPS is currently authorized for use in food contact materials with certain restrictions, such as a specific migration limit (SML) of 50 μg/kg (EU10/2011) [4]. However, similar to BPA, concerns regarding the obesogenic risk of BPS are increasing. Notably, perinatal BPS exposure has been discovered to heighten susceptibility to high-fat diet (HFD)-induced adipogenesis in recent years [5]. Perinatal exposure to Bisphenol S (BPS) has been reported to induce adipogenic effects in male mice offspring, particularly when subjected to a HFD [6]. This exposure resulted in overweight conditions, evidenced by increased body weight and elevated weights of the liver and epididymal white adipose tissue (epiWAT) [6,7]. Moreover, there was a notable increase in plasma triglyceride clearance [6], total cholesterol levels [8], and systolic blood pressure [8], along with the development of dyslipidemia [9]. At the molecular level, BPS exposure altered the expression of genes related to adipose tissue homeostasis and inflammatory pathways in liver tissues and epiWAT [5,7]. Additionally, it significantly affected genes involved in lipid and glucose metabolism[10]. These findings underscore BPS's potential risk within the DOHaD (Developmental Origins of Health and Disease) framework[11]. This suggests that changes in the gestational microenvironment during early development may contribute to the later onset of metabolic diseases. Moreover, it highlights the potential danger of BPS in unhealthy dietary patterns characterized by high caloric density and increased fat consumption.

Despite growing evidence linking perinatal BPS exposure to obesity, comprehensive investigations into how BPS affects offspring remain limited, often focusing on a narrow set of genes, metabolites, and tissues. BPS is detected in both breast milk and the umbilical cord, facilitating exposure to offspring via the placental barrier and entry into fetal circulation or through breastfeeding [12,13], potentially altering systemic metabolism. Systemic disruptions in metabolic homeostasis are key drivers of metabolic diseases. However, metabolite profiles, being the final product of complex molecular interactions, cannot be fully predicted by genomic, transcriptomic, or proteomic data due to the intricate feedback mechanisms [14]. In addition to systemic disruptions in metabolic homeostasis, the neonatal gut microbiome can be influenced by maternal factors through breastfeeding, and its role in obesity progression via microbiota-dependent mechanisms has gained significant attention [15,16]. The route of perinatal BPS exposure for offspring, whether through the placental barrier or breastfeeding, underscores the importance of developing a comprehensive atlas that integrates the multi-tissue metabolome and microbiome, to fully unravel the complex connections between perinatal BPS exposure and the development of metabolic diseases in offspring, particularly under high-caloric-density dietary conditions. To our knowledge, such a comprehensive atlas addressing these gaps remains limited.

This study aimed to elucidate the inclusive findings of previous research and address the knowledge gap regarding how BPS affects offspring across different organs, doses, and sexes. We investigated the impact of prenatal BPS exposure on adiposity and insulin resistance in HFD-fed offspring mice by integrating insights from both metabolomics and microbiomics. High-resolution mass spectrometry (HRMS)-based nontargeted metabolomics was employed to track perturbations in endogenous metabolism across 5 tissues: heart, liver, pancreas, white adipose tissue (WAT), and brown adipose tissue (BAT). Additionally, BPS-induced changes in the microbiome were measured using 16S rRNA sequencing. By combining metabolic interactions and microbiome shifts, the findings are expected to unveil the underlying health impacts of perinatal BPS exposure to HFD-induced adipogenesis, including remodeling profiles of the multi-tissue metabolome and microbiome, gender- and dose-related disturbances patterns and correlations among phenotypes, metabolome, and microbiome. Furthermore, this study aims to explore potential targets for early interventions.

2. Materials and methods

2.1. Animal experiments

All C57BL/6 mice were obtained from Anhe Yuan Biological Technology Co. (China). This work has received approval for research ethics from Jimei University (China) and a proof/certificate of approval is available upon request, complying with the "Guide for the Care and Use of Laboratory Animals" set by the National Institutes of Health.

The scheme of this study is illustrated in Fig. 1A. C57BL/6 pregnant mice (F0) were housed under controlled environmental conditions of 23 ± 1 ℃ temperature and 55 ± 5 % humidity. They were provided a standard diet (3.44 kcal/g, 12.95 % of kcal from fat, Beijing Keao Xielite Feed Co., Ltd., China) and maintained on a 12-hour light/dark cycle. To minimize BPS exposure outside of experimental procedures, the mice were accommodated in polystyrene cages equipped with glass bottles.

In the first batch (Batch I), 18 pregnant mice (F0), aged 10 weeks, were divided into three groups: control, low-dose (0.05 mg/kg/d of BPS), and high-dose (5 mg/kg/d of BPS) groups. The low dose of BPS was selected based on several considerations: (i) Relevance to pregnant women: Serum concentration of total bisphenols in pregnant women has been reported to reach a maximum of 144 ng/mL [17], corresponding to an approximate dose of 0.01 mg/kg in mice (assuming 8 % of mouse weight as blood volume). (ii) Occupational exposure relevance: In populations exposed to higher occupational BPA levels, median serum concentrations of BPA reached 101.94 μg/L [18], which is comparable to a dose of approximately 0.008 mg/kg in mice. (iii) Placental concentrations: BPA concentrations ranging from 1.0 to 104.9 ng/g (approximately 0.1 mg/kg) have been reported in human placental tissues [19]. (iv) Established tolerable daily intake (TDI): The TDI for BPA, determined by the European Food Safety Authority (EFSA) in 2006, is 0.05 mg/kg (EFSA-Q-2005–100) [20]. (v) Alignment with regulatory

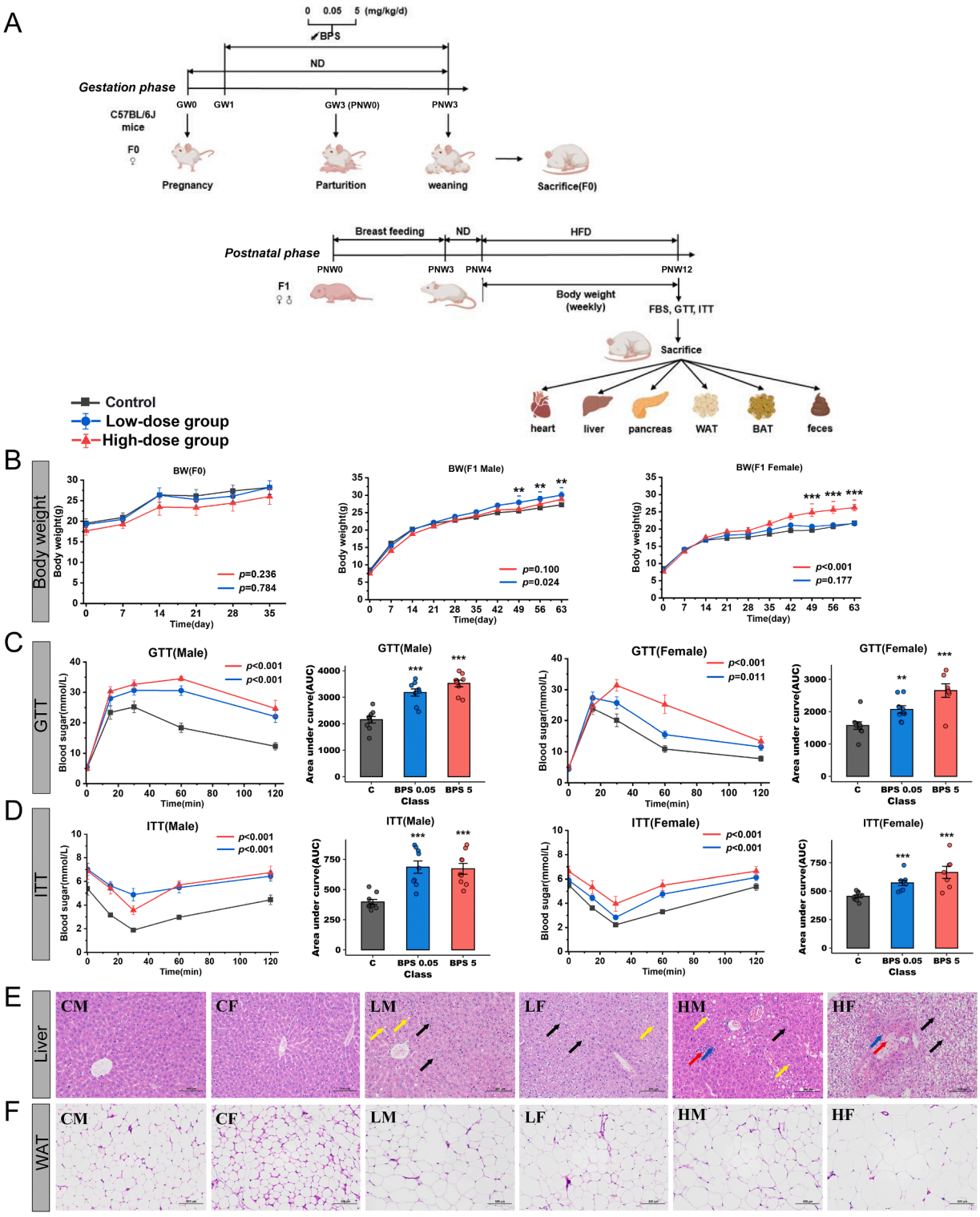

Fig. 1. Characterization of obesity and insulin resistance phenotypes in F1 mice. (A) Schematic overview of the experimental study design. (B) Body weight of F0 (n = 6 per group), F1 males (n = 9 per group), and F1 females (n = 9 per group, except the high-dose group which contains 7 females). (C) Blood glucose levels and area under the curve (AUC) following a glucose tolerance test (GTT) conducted in F1 males and females. (D) Blood glucose levels and AUC measured during an insulin tolerance test (ITT) in F1 males and females. For both GTT and ITT, n = 9 per group for F1 males and females, except for the high-dose group with 7 females. (E) and (F) Histopathological changes in the liver and WAT of F1 mice compared to controls (Hematoxylin and Eosin (H&E), original magnification × 200). CM (or CF), males (or females) in the control group. LM (or LF), males (or females) in the low-dose group. HM (or HF), males (or females) in the high-dose group. In the histopathological images of liver, black arrows indicate granular degeneration of hepatocytes, characterized by loose, lightly stained cytoplasm; yellow arrows indicate steatosis, characterized by vacuolated cytoplasm; red arrows indicate hepatocyte necrosis, characterized by karyopyknosis, karyorrhexis, or karyolysis; blue arrows indicate infiltration of granulocytes.

limits: This dose aligns with current regulatory restrictions, including the specific migration limit (SML) of 50 μg/kg (i.e., 0.05 mg/kg) for BPS, as authorized for use in food contact materials (EU10/2011) [4]. Therefore, the chosen low dose of 0.05 mg/kg/day is comparable to human exposure levels reported in specific sensitive populations. Additionally, By 2020, the EFSA reported a lowest no observed adverse effect level (NOAEL) for BPS of 20 mg/kg (EFSA-Q-2019–00299) [4]. Accordingly, a dose of 5 mg/kg/d was used in this study for the high-dose group. The BPS stock solution was prepared in DMSO, followed by dilution with physiological saline to generate the working solution (DMSO concentration not exceeding 0.1 % v/v). BPS exposure to F0 mice was administered via subcutaneous injection starting from the first week of gestation (GW1) and continued until post-natal week 3 of F1 offsprings (the end of lactation, PNW3). Control pregnant mice received a subcutaneous injection of an equivalent volume of physiological saline. To ensure precise control over the administered dosage of BPS while minimizing stress in pregnant female mice, BPS was administered to F0 mice via subcutaneous injection. The F1 offspring, however, were not injected with BPS. F1 offspring were exposed to BPS through the placental barrier and breastfeeding, closely mimicking the natural routes of BPS transmission from mother to offspring, thereby ensuring the ecological validity and relevance of subsequent analyses focused on the F1 generation. After F0 mice were exposed to BPS from GW1 to PNW3, they were finally sacrificed.

A total of 52 offspring (F1) from Batch I were kept for subsequent modeling. In each group, 18 F1 mice were kept as replicates, consisting of 9 males and 9 females (the high-dose group contains 7 females). After a 3-week lactation period, all F1 offspring were transitioned to a standard diet for a 1-week adaptive feeding period. Subsequently, at PNW4, they were shifted to a high-fat diet (5.24 kcal/g, 60 % of kcal from fat), based on Research Diets D12492 (USA), for a duration of 8 weeks. All F1 offspring from both maternal BPS exposure and control groups were subjected to the high-fat diet without additional BPS injection. All F1 offspring from both the maternal BPS exposure and control groups were administered a high-fat diet, with no subsequent BPS injections. At PNW12, two F1 mice from each dose and gender-specific group were randomly selected and sacrificed for histopathological analysis, while 41 mice were retained for subsequent metabolome and microbiome sample collection, with 14 F1 mice (7 males and 7 females) kept as replicates for each group, except for the high-dose group, which contained 6 females. Fecal samples were collected from the F1 mice via stress-induced defecation sampling method. Additionally, F1 mice tissues including the heart, liver, pancreas, white adipose tissue (WAT), and brown adipose tissue (BAT) were collected, rapidly washed in physiological saline, and then processed in liquid nitrogen before being stored at −80 ℃.

During the animal modeling process, the body weight of F0 and F1 mice was monitored on a weekly basis.

For validation of potential biomarker, a second cohort of mice (Batch II) was further utilized for modeling. Five pregnant mice (F0) received subcutaneous injections of a high dose of BPS (5 mg/kg/d). A total of 14 offspring (F1), comprising 7 males and 7 females, were retained for subsequent experiments, with none receiving BPS injections. Batch II was modeled using the same protocol as Batch I.

2.2. Fasting blood glucose, glucose and insulin tolerance tests

At the end of the experiment (PNW12), all F1 mice were firstly fasted overnight, and blood was collected to measure fasting blood glucose levels.

Glucose tolerance test (GTT) was performed on F1 mice that had been fasted for 6 hours, followed by an intraperitoneal injection of 2 g/kg glucose. Blood glucose levels were measured before (0 min) and after the injection (15, 30, 60, and 120 min).

Insulin tolerance test (ITT) was conducted on F1 mice that had been fasted for 6 hours, followed by an intraperitoneal injection of 0.75 IU/kg insulin. Blood glucose levels were measured before (0 min) and after the injection (0, 15, 30, 60, and 120 min).

2.3. Histopathological analysis

Histopathological changes in five mouse tissues from F1 mice, namely heart, liver, pancreas, WAT, and BAT, were examined after preparing paraffin-embedded sections and staining them with Hematoxylin and Eosin (H&E).

2.4. Fecal microbial community analysis

Fecal samples were collected from F1 mice for microbial community analysis following established methods [21]. Total genomic DNA was extracted from the fecal bacteria using the cetyltrimethylammonium bromide and sodium dodecyl sulfate method. DNA concentration and purity were assessed on 1 % agarose gels. DNA samples with a final concentration of 1 ng/μL were subjected to bacterial 16S rRNA gene amplification sequencing (V4 regions). The abundance and diversity of microbial taxa were determined using the Illumina NovaSeq 6000 platform (Novogene, Beijing, China). Library quality was evaluated with a Qubit (Thermo Scientific, USA) and Q PCR quantification.

Paired-end reads were assigned based on the sample's unique barcodes and trimmed to remove barcode and primer sequences. FLASH (v1.2.7) was used to merge overlapping paired-end reads. Raw splicing sequences were filtered to obtain clean, high-quality tags through the QIIME (v1.9.1) quality control process. Chimeric sequences were identified and removed using the Uparse algorithm, based on comparison with the Gold database, to obtain effective tags. Sequences with similarities of at least 97 % were classified as the same operational taxonomic unit (OTU). The representative sequence of each OTU was annotated with corresponding taxonomic information according to the SSUrRNA Database using the Ribosomal Database Project Classifier algorithm. OTU abundance was normalized based on the sequence number of the sample with the fewest sequences. The data were then defined as the relative abundance and used for subsequent statistical analysis.

2.5. Non-targeted metabolomics analysis on multiple mouse tissues

The deep-frozen tissue from each replicate of F1 mice was accurately weighed (approximately 15 mg) and subsequently transferred to an Eppendorf tube. Non-targeted metabolomics study was conducted on multiple mouse tissues following our previously published method [22]. Metabolite extracts from tissues were analyzed using ACQUITY ultra-performance liquid chromatography (UPLC, Waters, USA) coupled with Q-Exactive HF mass spectrometry (Thermo Fisher Scientific, USA) in both positive and negative analysis modes to acquire metabolomics profiling. Detailed information on the metabolomics analysis, including metabolome extraction, equipment, and parameters of metabolomics acquisition, is provided in the Supporting Information.

Quality control (QC) samples were obtained from pooled metabolic extracts and prepared as real samples. These QC samples were analyzed every 10 injections during the entire run to monitor the robustness of the analysis.

2.6. Data processing and statistics

Approximately 2000 metabolite standards were pre-analyzed by our collaborator to develop an in-house database [23]. Metabolites were then identified using this standards database, leveraging accurate m/z values, tandem mass spectrometry (MS/MS) fragmentation patterns, and retention times. Additionally, the mzCloud software (Thermo Fisher Scientific, USA) was utilized to assist the identification process by providing comprehensive MS and MS/MS information. The quantification of metabolites was subsequently performed using Trace Finder software (Thermo Fisher Scientific, USA) with a retention time extraction window of ± 15 s and a m/z tolerance of ± 10 ppm. Peak checking

and noise removal were carried out to reduce errors.

Prior to statistical analysis, the peak areas of metabolites in each sample were first normalized to tissue weight, and then to the peak areas of internal standards. Peak refinement was performed using the 80 % rule, and metabolites with a %RSD more than 30 % in QC samples were also removed. The processed dataset was then submitted for subsequent statistical analysis. Detailed information on statistical analysis is provided in the Supporting Information.

2.7. Proteomics validation on adipose tissues

In the comparison across multiple tissues based on the entire atlas, BAT and WAT emerged as potential target tissues. Given the comparable changes observed between the low- and high-dose groups, and the heightened concerns about the risks associated with low-dose BPS exposure, adipose tissues from the low-dose group were selected for proteomic analysis of key proteins.

The protein extraction was conducted by using the protein extraction kit (Catalog # AT-022, Invent) according to the manufacturer's protocol. The protein concentration was quantified using BCA assay kit (Cat # 23225; Thermo Fisher Scientific, Inc.). A filter-aided sample preparation (FASP) method was used for protein digestion [24]. The MS analysis was performed according to our recent study [25]. Briefly, separation was performed on a 25 cm PepMap analytical column (ThermoFisher Scientific). MS1 spectra were obtained in the Orbitrap. The collection of MS2 spectra was completed in the linear ion trap. Proteome Discoverer Software (version 2.5, San Jose, CA) was used to process raw files for detecting features, searching databases and quantifying

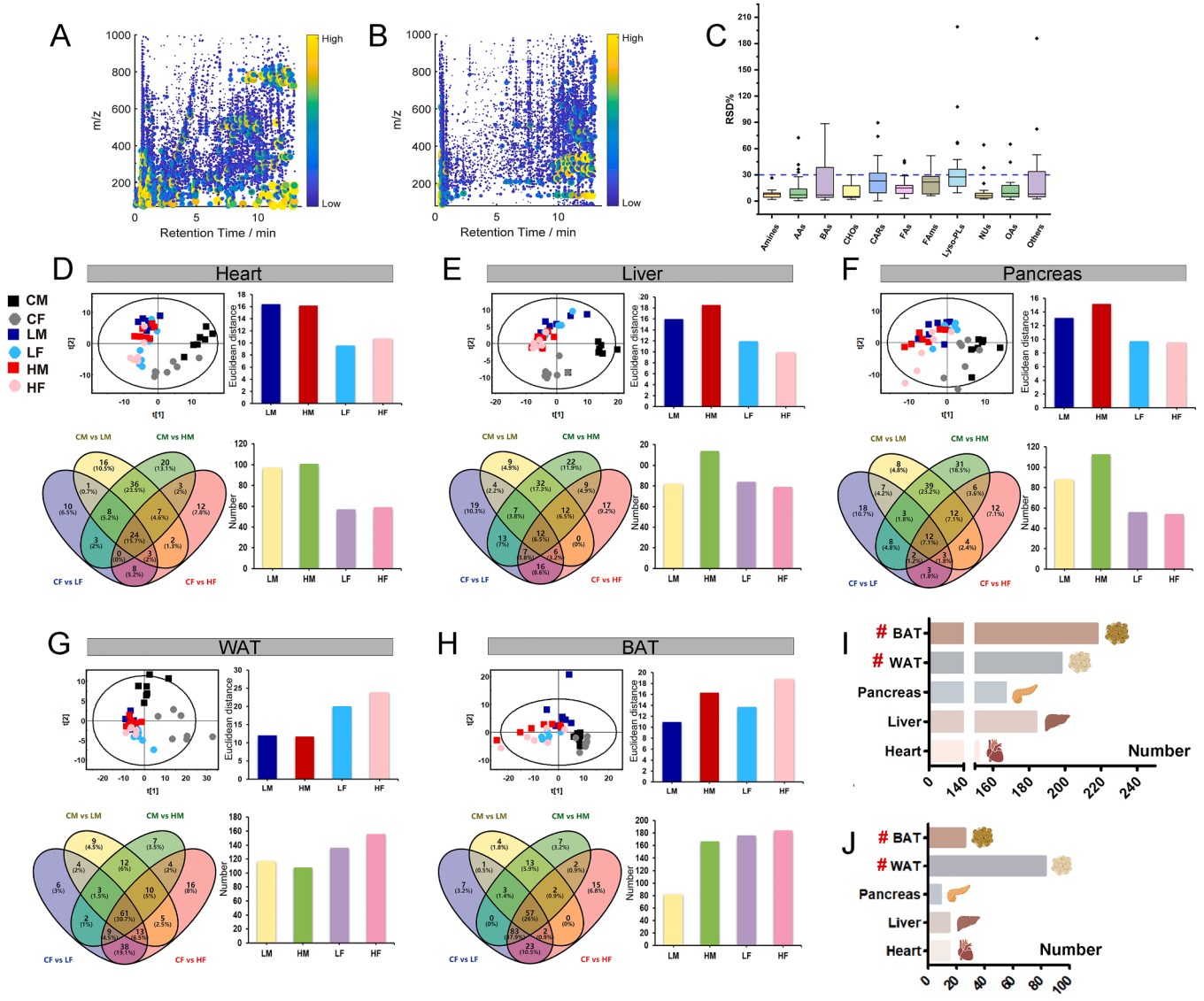

Fig. 2. Metabolomics atlas of multiple tissues following BPS exposure. (A) and (B) Representative metabolomics profiles in positive and negative ionization modes, respectively. (C) Distribution of total %RSD across different metabolite classes. (D)-(H) Multivariate and univariate analyses based on metabolomic profiling of heart, liver, pancreas, WAT, and BAT. In each panel, the top two sub-figures display the score plot from PLS-DA followed by a histogram representing Euclidean distance statistics; the bottom two sub-figures show a Venn diagram illustrating univariate comparisons between BPS-exposed groups and gender-matched controls ($p < 0.05$, Wilcoxon-Mann-Whitney test) and a subsequent histogram of significant differential metabolites. For metabolomics study, 14 F1 mice (7 males and 7 females) kept as replicates for each group, except for the high-dose group, which contained 6 females. (I) A bar chart illustrating significant differences in the number of metabolites across five tissues. The union of metabolite differences between different gender and dose groups is used to represent the typical set of metabolic differences in each tissue. (J) A bar chart displaying the number of metabolites significantly correlated with phenotypic traits across five tissues. Significant differential metabolites that exhibit strong correlations with various phenotypic indicators, including body weight (BW), fasting blood glucose (FBG), GTT, and ITT (Spearman correlation coefficient $|Cij| > 0.6$, $p < 0.05$, two-tailed test), are combined to form the set of significant phenotype-associated differential metabolites for each tissue.

proteins/peptides. MS/MS spectra were searched against the UniProt mouse database (downloaded on June 24th, 2022, containing 55,286 entries). Methionine oxidation and N-terminal protein acetylation were chosen as variable modifications, while the carbamidomethylation of cysteine residues was regarded as a fixed modification.

Detailed information on the proteomics analysis, including protein extraction, equipment, parameters of proteomics acquisition and data analysis is provided in the Supporting Information.

3. Results

3.1. Obesity and insulin resistance phenotypes in F1 mice

Compared to controls, F1 males from the low-dose group and F1 females from the high-dose group exhibited a significant increase in body weight (Fig. 1B), while F0 mice showed no significant differences in body weight.

In terms of glucose metabolism, no significant changes were observed in fasting blood glucose levels between the control and low/high-dose groups in F1 mice (Figure S1). However, the areas under the curve (AUC) for both GTT and ITT tests were significantly elevated in F1 males and females (Fig. 1C and D), indicating a significant reduction in glucose processing efficiency and insulin sensitivity in F1 mice.

Histopathological changes in the tissues (heart, liver, pancreas, WAT and BAT) of F1 mice were examined in comparison to controls. In the liver, BPS exposure caused cytoplasmic loosening and hypochromasia, with numerous hepatocytes displaying vacuolation. There was a dose-dependent increase in the incidence of granular degeneration, steatosis, and hepatocyte necrosis (Fig. 1E). In the WAT, BPS exposure also resulted in dose-dependent adipocyte enlargement (Fig. 1F). No significant pathological changes were observed in other tissues (Figure S2).

3.2. Metabolome atlas of multiple tissues following BPS exposure

A metabolome atlas of multiple tissues from F1 mice was acquired to comprehensively explore the influence of perinatal BPS exposure (Fig. 2A and B). A total of 361 metabolites from a wide spectrum of categories were finally identified, including amino acids (AA), carbohydrates (CHO), nucleotides (NU), organic acids (OA), bile acids (BA), carnitines (CAR), fatty acids (FA), fatty acid amide (FAm), lysophosphatidylphospholipid (Lyso-PL), and amines (Am), among others (Figure S3, Table S1). The stability and reproducibility of the metabolomics profiling was examined by evaluating QC samples and was confirmed to be satisfactory for complex biological samples (Figs. 2C and S3). Detailed information on these identified metabolites and QC evaluation results are provided in the Supporting Information.

Multivariate analyses based on partial least squares discriminant analysis (PLS-DA) and subsequent Euclidean distance statistics were performed to obtain an overview of the metabolic disturbances (Fig. 2D-H). Euclidean distance was calculated between each BPS exposure group and the gender-matched controls based on the coordinates in the PLS-DA score plot to quantify their differences. BPS-related changes were clearly visible across multiple tissues, as demonstrated by the obvious separation trend between exposure groups and controls on the PLS-DA score plots. In terms of gender, F1 males exhibited greater disturbances in the metabolome atlas of the heart, liver and pancreas compared to females, while F1 females were observed with more remarkable changes in BAT and WAT metabolome atlas. Furthermore, similar metabolic changes between high and low dose groups were identified in most tissues, indicating the non-negligible disruptions even at low dose BPS.

Subsequently, univariate statistical analyses using the Wilcoxon-Mann-Whitney test were performed to compare each BPS exposure group with the gender-matched controls, in order to identify significantly changed metabolites ($p < 0.05$, Fig. 2D-H). The analysis revealed that BAT and WAT exhibited the highest number of significant differential metabolites (Fig. 2I, Table S2). Additionally, Spearman correlation analyses were conducted to explore the relationship between metabolome from each tissue and phenotypic measures, including body weight, fasting blood glucose, GTT, and ITT (Table S3). BAT and WAT displayed the greatest number of metabolites significantly correlated with these phenotypic measures, with a Spearman correlation coefficient |Cij| exceeding 0.6 and a two-tailed test p-value less than 0.05 (Fig. 2J). Consequently, BAT and WAT were identified as potential target tissues for investigating the effects of BPS exposure.

3.3. Remodeling patterns of metabolome across multiple tissues

To specify the changes within each metabolite class, the significant differential metabolites were normalized to the total number of metabolites in each class for enrichment analysis (Figs. 3A, B and S4). The proportion of significant differential changes in each metabolite class in BAT and WAT was more remarkable than in other tissue. Notably, most metabolites in WAT were significantly decreased, whereas those in BAT were significantly increased.

The enrichment overview of metabolites demonstrating significant changes in the metabolome (Table S2) or exhibiting significant correlations with phenotypic measures (Table S3) was presented across various tissue types (Fig. 3C and D). CARs emerged as the top metabolite class with remarkable metabolic changes (top 3) across all tissue types (Fig. 3C), whereas AAs were identified as the top metabolite class with noteworthy correlations with phenotypic measures (top 5) in all tissue types (Fig. 3D).

Furthermore, remodeling patterns of significant differential metabolites were illustrated using heat maps (Figure S5). Inverse change patterns were observed between BAT and WAT, indicating tissue-specific metabolome remodeling in response to BPS exposure. Specifically, most BAs and CARs were decreased in the heart and WAT, Lyso-PLs were decreased in the pancreas, while AAs, CARs, FAms and Lyso-PLs were increased in BAT.

These significant differential metabolites across multiple tissues indicated the disturbances in metabolic pathways, primarily including linoleic acid metabolism, alanine, aspartate and glutamate metabolism, phenylalanine, tyrosine and tryptophan biosynthesis, and D-glutamine and D-glutamate metabolism (Fig. 3E).

3.4. Gender- and dose-related metabolome disturbances following BPS exposure

After dividing the exposed subjects by gender-matched controls (i.e., the baseline substrate), a two-way ANOVA was used to find metabolome disruptions associated to both gender and dosage following BPS exposure.

With the exception of the pancreas, most tissue types showed extensive gender-related alterations across almost all metabolite classes (Fig. 3F). Fifteen major gender-related difference metabolites including AAs, NUs, CHOs, OAs, and Ams were found throughout tissues (Figure S6). In contrast, dose-related metabolome changes involving AAs, NUs, CHOs, FAs, CARs, and OAs were exclusively significant in the liver (Fig. 3G).

3.5. Identification of potential metabolite biomarkers

To capture the most critical metabolic differential features, exposure groups were compared to gender-matched controls for biomarker discovery. Firstly, the intersection of representative significant differential metabolites meeting multivariable significance (VIP > 1), univariate significance ($p < 0.05$, FDR < 0.1, ratio > 2), and stringent reproducibility criteria (%RSD in QC < 20 %) was identified. Then, these metabolites were correlated with obesity/insulin resistance phenotypes (i.e., ITT and GTT). Significant correlations with obesity/insulin resistance phenotypes were found for the amino acid ergothioneine (EGT) from the heart, WAT, and BAT; the fatty acids FFA 24:5 from the heart and liver,

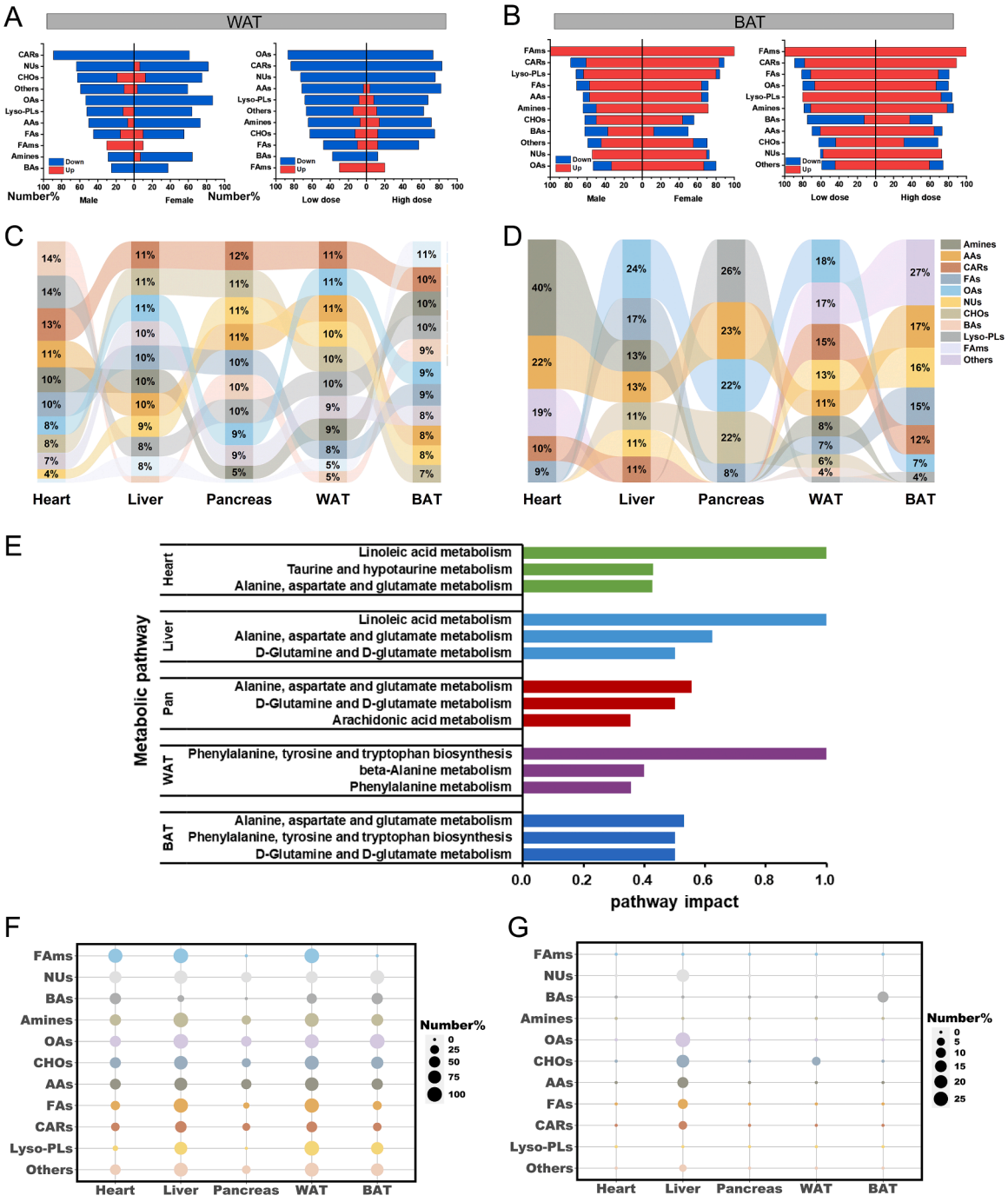

Fig. 3. Remodeling patterns of the metabolome. (A) Enrichment analysis of significant differential metabolites in WAT. The histogram represents the percentage of significant differential metabolites, with the number of metabolites significantly altered between gender groups (left panel) or exposure dosage groups (right panel) normalized to the total number of metabolites identified within each class. (B) Enrichment analysis of significant differential metabolites in BAT. (C) Sankey diagram illustrating the changes in the percentage of significant differential metabolites within each metabolite class across different tissues. (D) Sankey diagram showing the changes in the percentage of metabolites with significant correlations to phenotypic measures within each metabolite class across various tissues. (E) Disturbances in metabolic pathways based on significant differential metabolites enriched across multiple tissues. (F) Gender-related disturbances in the metabolome following BPS exposure. The number of metabolites significantly altered between gender groups is normalized to the total number of metabolites identified within each class. (G) Dose-related disturbances in the metabolome following BPS exposure.

and FFA 20:5 from the liver and pancreas; the carnitine (R)-3-hydroxybutyrylcarnitine from the pancreas; and (+,-)12(13)-DiHOME from the heart (Spearman correlation coefficient $|Cij| > 0.6$ and $p < 0.05$, Figure S7). These metabolites were finally identified as potential biomarkers, indicating the effects of perinatal BPS exposure in inducing obesity and insulin resistance in offspring (Figure S8). They demonstrated excellent performance in distinguishing controls from exposure groups, with an area under the ROC curve (AUC) value greater than 0.9 (Figure S9, Table S4).

Furthermore, these potential metabolite biomarkers were validated in discriminating exposure samples of batch II from controls, achieving similarly satisfactory performance with an AUC value greater than 0.75 (Figure S10, Table S4).

3.6. Changes in fecal microbial community composition

In addition to the metabolome atlas of multiple tissues, the 16S rRNA data from F1 mice were analyzed to depict the comprehensive effects of BPS exposure by examining changes in the fecal microbial community composition. Principal co-ordinates analysis (PCoA) revealed that the fecal microbial community structure of both low- and high-dose groups differed greatly from that of the control group (Fig. 4A). Remarkably, even the low-dose group exhibited changes similar to those observed in the high-dose group.

Compared to the control group, the exposure groups exhibited an increased Firmicutes/Bacteroidota (F/B) ratio at the phylum level. At the family level, the exposure groups demonstrated a decreased abundance of Muribaculaceae and Pseudomonadaceae, while the abundance of Erysipelotrichaceae and Atopobiaceae increased (Fig. 4B and C).

Furthermore, exposure groups were compared to gender-matched controls to identify significant changes in fecal microbial community composition at the species level ($p < 0.05$, Figure S11). A total of 29 significant differential microbiota were identified in BPS groups (Table S5). Perinatal BPS exposure induced more pronounced changes in the microbial abundance of F1 males compared to females. Additionally, the low-dose group exhibited changes similar in magnitude to those observed in the high-dose group.

A PICRUSt (Phylogenetic Investigation of Communities by Reconstruction of Unobserved States) analysis was conducted to predict the functional potential of the microbial community in the BPS group (Fig. 4D). The pathway annotation revealed that 46.91 % of the enriched genes were associated with metabolism, followed by pathways related to genetic information processing (19.57 %) and environmental information processing (15.01 %). Notably, amino acid metabolism,

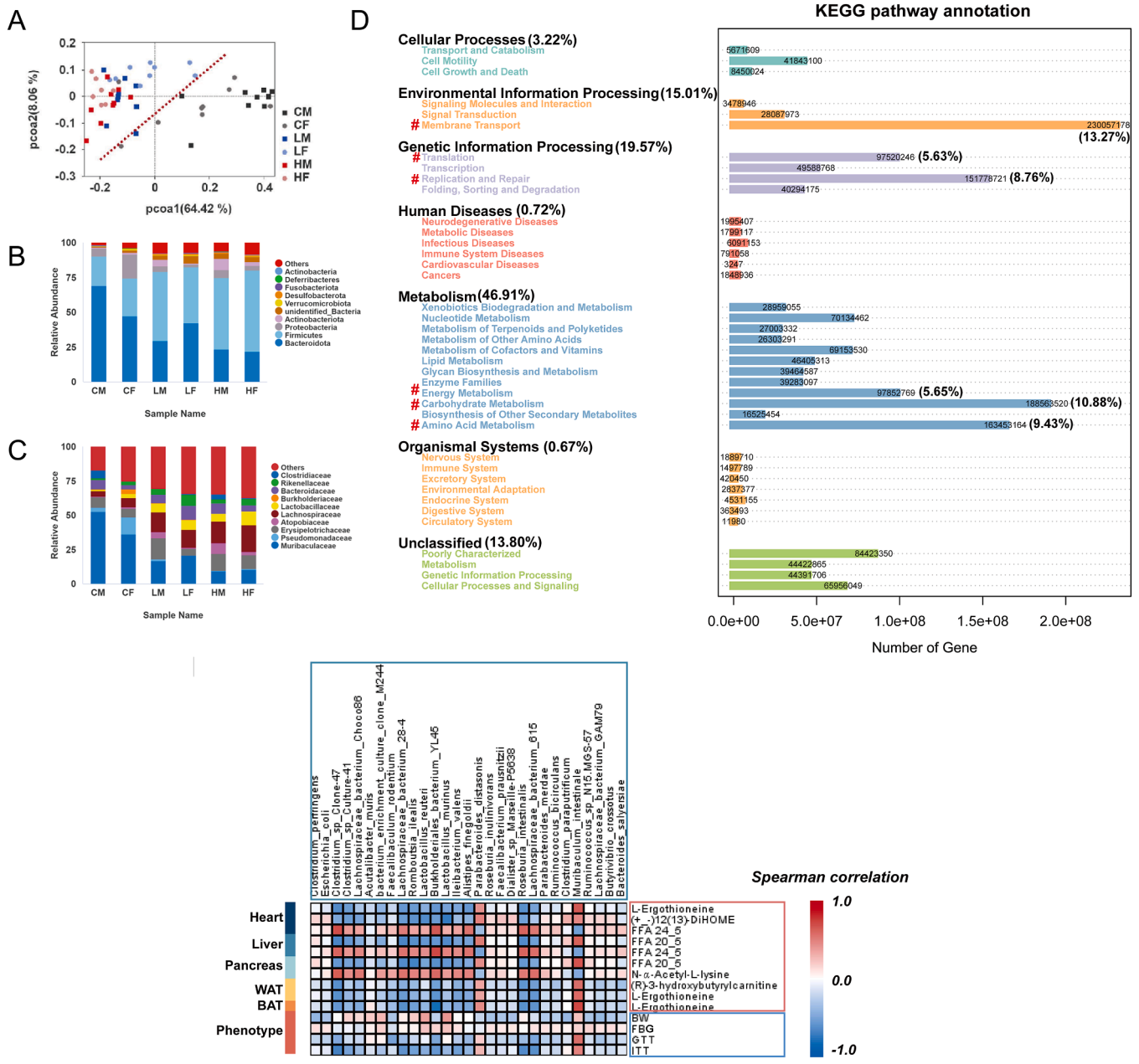

Fig. 4. Changes in fecal microbial community composition. (A) Principal Co-ordinates analysis (PCoA) illustrating the overall variation in microbial community composition across groups. For fecal microbial community analysis, 14 F1 mice (7 males and 7 females) kept as replicates for each group, except for the high-dose group, which contained 6 females. (B) Microbial composition at the phylum level in each group. (C) Microbial composition at the family level in each group. (D) Results of the pathway annotation. (E) Heat map depicting the correlations between metabolite biomarkers, phenotypic traits, and significant differential microbiota.

carbohydrate metabolism, energy metabolism, membrane transport, translation, and replication and repair were identified as the primary pathways with the highest enrichment, each comprising more than 5.0 % of the total enriched genes.

3.7. Correlation among phenotypes, metabolome, and microbiome

Given the functional potential in the microbial community, which exhibited the highest enrichment in metabolism-related pathways, the correlation among phenotypes, metabolome, and microbiome was further investigated (Table S6).

Most differential microbiota, which exhibited significant differences in abundance when comparing exposure groups to controls, were significantly negatively correlated with metabolite biomarkers and phenotypes. In contrast, *Parabacteroides-distasonis* and *Muribaculum-intestinale* tended to show more significant positive correlations. Additionally, FFA 24:5 (in heart and liver) and N-α-Acetyl-Lysine (in pancreas) were significantly positively correlated with most differential microbiota.

In summary, our study identified that approximately 50 % of the differential microbiota were significantly correlated with phenotypes and potential metabolite biomarkers across multiple tissues. A total of 9 representative differential microbiota, including *Burkholderiales-bacterium-YL45*, *Lactobacillus-reuteri*, *Lactobacillus-murinus*, *Lachnospiraceae-bacterium-28–4*, *Lachnospiraceae-bacterium-615*, *Roseburia-intestinalis*, *Romboutsia-ilealis*, *Clostridium-sp-Clone-47* and *Clostridium-sp-Clone-47* (Figure S12), showed the most significant correlations (Spearman correlation coefficient $|Cij| > 0.6$ and $p < 0.05$, Fig. 4E). These microbiotas predominantly originated from the genera *Lachnospira*, *Lactobacillus*, and *Clostridium*, indicating a specific tendency of the microbiome in response to BPS exposure and suggesting a potential relationship to AAs, FAs and CARs related metabolism.

4. Discussion

In this study, key phenotypes, including body weight, fasting blood glucose, glucose and insulin tolerance tests, as well as histopathological changes, were selected to confirm our model, given that other indicators, such as plasma parameters regarding dyslipidemia, have been reported in previous studies [9]. Therefore, our aim is to explore the molecular mechanisms underlying the effects of perinatal BPS exposure by constructing a comprehensive atlas of metabolome and microbiome shifts across multiple tissues and fecal samples.

Consistent with previous findings, our study observed the onset of obesity in F1 mice following perinatal BPS exposure. Especially, both male and female F1 offspring exhibited significant reduction in glucose and insulin tolerance. The metabolome/microbiome atlas indicated a gender-dependent response to perinatal BPS exposure. Compared to females, F1 males exhibited more pronounced changes in the metabolome across multiple tissues (heart, liver and pancreas) as well as greater alterations in microbial abundance. Given that hormones are potent regulators of energy metabolism [26], and considering the estrogenic and antiandrogenic properties of BPS, this gender-dependent pattern suggests a potentially more pronounced influence of BPS on males. Conversely, the BPS-induced disruption of estrogen homeostasis in females may be relatively modest in the context of endogenous estrogen pools [9].

Furthermore, although the influence of low-dose BPS exposure was slightly weaker than that of high-dose exposure across the entire atlas, their comparable changes observed indicated the nonnegligible endocrine-disrupting activities of low-dose BPS. The emergence of nonmonotonic dose-response patterns would involve the presence of nonmonotonic endocrine-disrupting activities, likely due to the complex dynamics of receptor occupancy and saturation, as has been reported for several other environmental endocrine disrupters [27].

4.1. Metabolic competition between WAT and BAT

By integrating the following factors: i) class enrichment of significant differential metabolites, ii) pathway enrichment analysis of these metabolites, iii) their correlations with phenotypic measures, and iv) significant functional alterations in the microbial community, amino acid, fatty acid and carnitine metabolism were identified as the key disturbances in response to perinatal BPS exposure (Fig. 5A). Notably, in our comprehensive atlas, BAT and WAT emerged as potential target tissues. This identification was based on the top metabolome disturbances observed in these tissues and their strong correlation with phenotypic measures.

Carnitines function as carriers for transporting fatty acids, facilitating the entry of long-chain fatty acids into mitochondria for oxidative breakdown and energy production [28]. Following perinatal BPS exposure, the observed downregulation of carnitines in the liver and WAT of F1 offspring on a high-fat diet may impede the entry of fatty acids into mitochondria for β-oxidation, ultimately resulting in fat accumulation in the WAT. This observation is consistent with the enlarged white adipocytes found in the F1 offspring within the BPS exposure group. Such fat accumulation is associated with an increased risk of metabolic diseases [29].

Unexpectedly, BPS exposure induced a significant upregulation of fatty acids and carnitines in BAT. During triglyceride lipolysis, the released fatty acids are oxidized in mitochondria and activate uncoupling protein 1 (UCP1), thereby initiating thermogenesis [30]. UCP1 is a hallmark thermogenic protein that boosts energy expenditure within the body [31]. For further validate these findings, we conducted proteomics analysis on BAT and confirmed a significant upregulation of the thermogenic protein UCP1 in the exposure group (Fig. 5B), accompanied by a significant downregulation of the glucose transporter (GLUT4) (Fig. 5C). These results suggest that perinatal BPS exposure may reduce glucose uptake in brown adipocytes of F1 offspring, while free fatty acids are transported into mitochondria via acylcarnitine, where they are oxidized and activate UCP1, thereby promoting thermogenesis.

In summary, the fat accumulation of WAT, combined with the enhanced thermogenesis in BAT, indicates the existence of a compensatory balance mechanism. The obesity/insulin resistance observed in F1 offspring following perinatal BPS exposure appears to be closely associated with the disruption of this energy balance. Consequently, the unanticipated competition between WAT and BAT in response to BPS, characterized by their respective roles in fat storage and utilization, may play a significant role in contributing to the observed obesity and insulin resistance phenotype (Fig. 5D).

Moreover, analysis of key differentially enriched pathways revealed a significant downregulation of alanine, aspartate, glutamate, and glutamine in the WAT of F1 offspring in response to perinatal BPS exposure. Beyond their established roles in protein synthesis, these amino acids can undergo transamination, facilitating the removal of the α-amino group and producing organic acids that act as substrates for the tricarboxylic acid (TCA) cycle, thereby contributing to energy production. Notably, obesity-related insulin resistance has been associated with a reduced glutamine-to-glutamate ratio in WAT [32]. Recent reports have highlighted WAT glutamine turnover as a critical determinant of energy expenditure and metabolic health [32]. Consistent with our findings of decreased WAT glutamine-to-glutamate ratios (Figure S13), this study highlights the profound effects of perinatal BPS exposure on the reprogramming of energy metabolism in the offspring.

4.2. Insights from microbiome shifts

Recent research has demonstrated that gut microbiota serves as a critical internal environmental factor in the development of obesity and type 2 diabetes [15,16]. In this study, approximately 50 % of the differential microbiota, which showed significant correlations with metabolite biomarkers and phenotypes, were predominantly derived

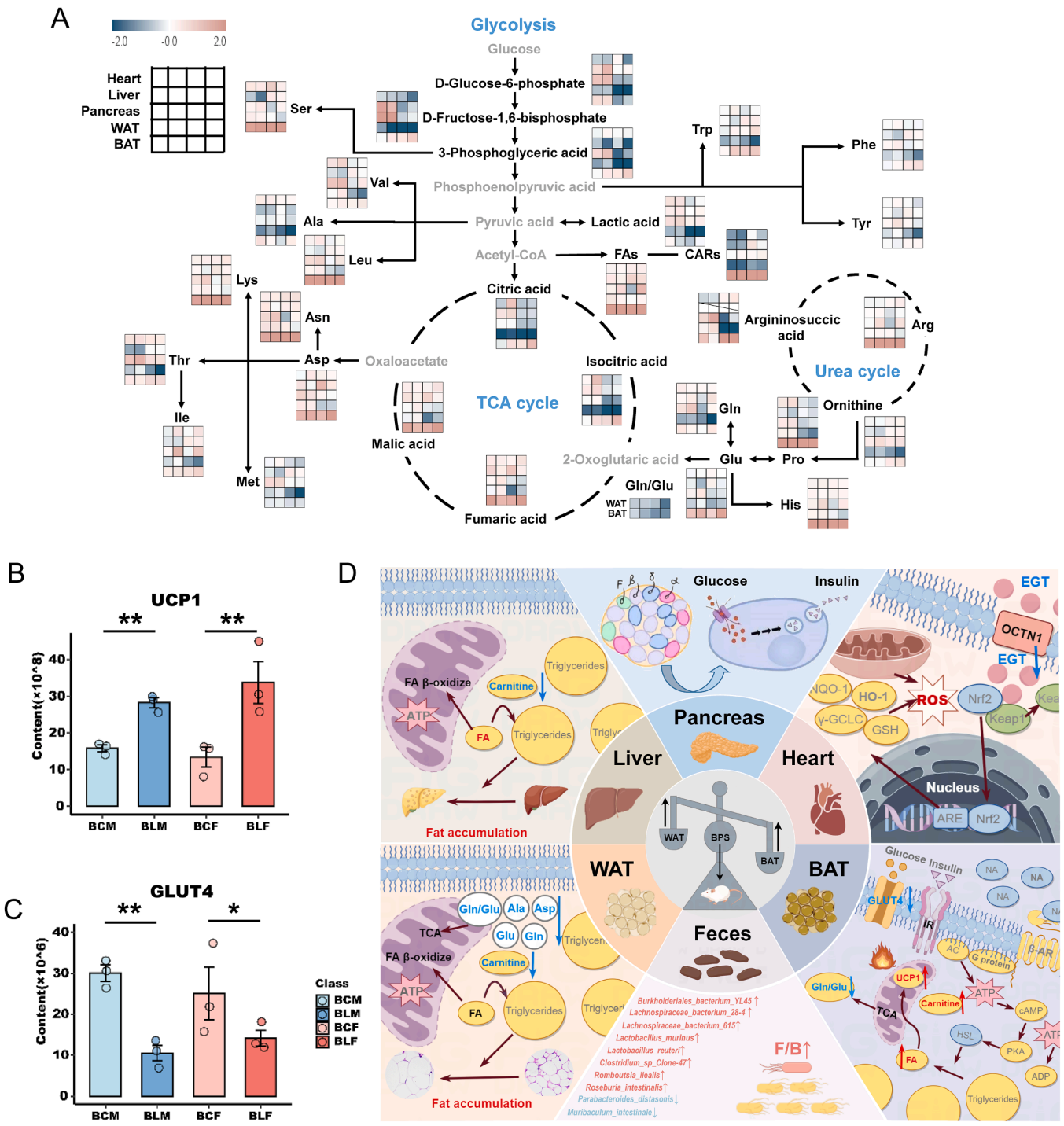

Fig. 5. Overview of disturbances caused by perinatal BPS exposure in high-fat diet-fed mice. (A) Schematic diagram of amino acid, fatty acid, and carnitine metabolic pathways. The heat map illustrates the relative abundance of metabolites in various tissues after normalizing the exposed subjects to their gender-matched controls (i.e., using the controls as the baseline), followed by log scaling. (B) and (C) Protein expression levels of UCP1 and GLUT4 in BAT across experimental groups. * : $0.01 < p < 0.05$, * *: $0.001 < p < 0.01$, * ** : $p < 0.001$. (D) Comprehensive atlas illustrating key shifts in the metabolome and microbiome across multiple tissues in response to perinatal BPS exposure.

from the genera *Lachnospira*, *Lactobacillus*, and *Clostridium*.

In F1 offspring, *Lachnospiraceae-bacterium-28–4* and *Lachnospiraceae-bacterium-615* (*Lachnospira*), *Lactobacillus-reuteri* and *Lactobacillus-murinus* (*Lactobacillus*) and *Clostridium-sp-Clone-47* (*Clostridium*) were significantly upregulated in response to perinatal BPS exposure (Figure S12). *Lachnospiraceae-bacterium-28–4* is linked to butyrate production, a process known to reduce food intake and attenuate high-fat diet-induced weight gain [33]. *Lactobacillus* species have been shown to lower blood glucose levels by modulating autonomic nerve transmission to stimulate insulin secretion [34], as well as to improve insulin resistance and insulin signaling pathways in the liver, thereby maintaining plasma insulin levels [35,36]. Additionally, *Lactobacillus-reuteri* exerts anti-obesity effects by inhibiting the expression of PPAR-γ, Acc1, and Fas in adipocytes, and Cyp7a1 in the liver [37]. *Clostridium* species can prevent weight gain by inhibiting the intestinal absorption of fats through downregulation of the CD36 gene expression [38]. The marked

upregulation of these beneficial bacteria in the BPS exposure group may therefore indicate a negative feedback resistance mechanism triggered by BPS-induced obesity and insulin resistance (Fig. 5D).

In addition to the findings in the metabolome of adipose tissues and the microbiome of feces, the significant decrease of ergothioneine (EGT) in the heart warrants attention. EGT, a natural thiourea derivative of histidine, is a low molecular weight thiol with antioxidant, anti-inflammatory, and detoxifying properties, potentially providing protection against oxidative stress [39]. Recent studies have shown that higher EGT levels serve as an independent marker of reduced risk for cardiometabolic disease and mortality in humans [40,41]. In the present study, EGT was also identified as a potential biomarker in the heart, with its significant reduction suggesting that BPS exposure may be linked to an increased risk of cardiometabolic disease in the offspring (Fig. 5D).

It is important to acknowledge that the limited dose groups used in this study. Future studies should assess the toxicity and no-effect levels of BPS across a broader range of doses relevant to human exposure. Moreover, even though our analysis focused on the F1 offspring to investigate effects induced by perinatal BPS exposure, differences in BPS absorption efficiency across various administration methods for F0 pregnant mice, such as subcutaneous injection, oral administration and intragastric administration, merit further investigation. Future studies should consider measuring BPS concentrations in multiple tissues and in serum/plasma to gain a comprehensive understanding of BPS distribution and metabolism.

5. Conclusion

In conclusion, the disturbances identified from the metabolome and microbiome atlas were strongly correlated. The microbial community from the BPS groups exhibited the highest functional enrichment in metabolism-related pathways, with a particular emphasis on amino acid metabolism, carbohydrate metabolism, and energy metabolism. These comprehensive disruptions in the atlas indicated that perinatal exposure to BPS in F1 offspring may impair the transport of fatty acids into mitochondria for β-oxidation by reducing carnitine carriers, ultimately contributing to fat accumulation in WAT. Unexpectedly, a resistance mechanism was indicated by the mobilization of compensatory thermogenesis in BAT and a significant increase in beneficial commensal bacteria. Our findings provide novel insights into the unexpected resistance mechanism triggered by perinatal BPS exposure and the resulting metabolic imbalance that contributes to obesity and insulin resistance in offspring, highlighting the potential for early interventions targeting key metabolic pathways and gut flora to reverse these adverse outcomes.

Environmental implication

Bisphenol S (BPS) is a substitute for Bisphenol A (BPA) in 'BPA-free' products. While perinatal BPS exposure is suspected to increase susceptibility to diet-induced adipogenesis, its effects on offspring across organs, doses, and sexes remain largely unknown. This study examined effects of perinatal BPS exposure on adiposity and insulin resistance in C57BL/6 offspring fed a high-fat diet (HFD). We conducted phenotypic assessments and created an atlas of metabolome and microbiome shifts across heart, liver, pancreas, WAT, BAT, and feces, validated by proteomics. Our findings aimed to provide novel insights into how BPS affects offspring and identify potential biomarkers for early intervention.

CRediT authorship contribution statement

Shuyin Li: Writing – original draft, Investigation. **Jun Zeng:** Writing – original draft, Project administration, Investigation. **Philippe Schmitt-Kopplin:** Writing – review & editing. **Shen Zhang:** Resources, Investigation. **Jiayi Lin:** Investigation. **Haoyue Song:** Investigation. **Longhua Gao:** Writing – original draft, Data curation.

Declaration of Competing Interest

The authors declare that they have no known competing financial interests or personal relationships that could have appeared to influence the work reported in this paper.

Acknowledgements

The study has been supported by Natural Science Foundation of Fujian Province of China (Grants No. 2022J01330), Natural Science Foundation of Xiamen City of China (Grants No. 3502Z20227208), Reproductive and Genetic Hospital of CITIC-XIANGYA (YNXM-202211), Hunan Provincial Grant for Innovative Province Construction (2019SK4012), Hundred Youth Talents Program of Hunan Province and China Scholarship Council (202308350047).

Appendix A. Supporting information

Supplementary data associated with this article can be found in the online version at doi:10.1016/j.jhazmat.2024.136895.Supporting Information: Chemicals and reagents, Metabolome extraction, Non-targeted metabolomics analysis of multi- mouse tissues, Data processing and statistics, Proteomics validation on adipose tissues, Table S1-S6, and Figure S1-S13. The mass spectrometry data of the current study are available in the Metabolomics Workbench (http://www.metabolomicsworkbench.org/) repository (Study ID ST003400, Data Track ID 5075).

References

[1] Heindel, J.J., Blumberg, B., 2019. Environmental obesogens: mechanisms and controversies. In: Insel, P.A. (Ed.), Annual review of pharmacology and toxicology. Annual Reviews, Palo Alto, pp. 89–106. https://doi.org/10.1146/annurev-pharmtox-010818-021304.

[2] Varghese, S.V., Hall, J.M., 2023. Bisphenol A substitutes and obesity: a review of the epidemiology and pathophysiology. Front Endocrinol 14. https://doi.org/10.3389/fendo.2023.1155694.

[3] Wu, L.H., Zhang, X.M., Wang, F., Gao, C.J., Chen, D., Palumbo, J.R., et al., 2018. Occurrence of bisphenol S in the environment and implications for human exposure: a short review. Sci Total Environ 615, 87–98. https://doi.org/10.1016/j.scitotenv.2017.09.194.

[4] FitzGerald, R., Loveren, H.V., Civitella, C., Castoldi, A.F., Bernasconi, G., 2020. Assessment of new information on Bisphenol S (BPS) submitted in response to the Decision 1 under REACH Regulation (EC) No 1907/2006. EFSA Support Publ 17 (4). https://doi.org/10.2903/sp.efsa.2020.EN-1844.

[5] Ahn, Y.A., Baek, H., Choi, M., Park, J., Son, S.J., Seo, H.J., et al., 2020. Adipogenic effects of prenatal exposure to bisphenol S (BPS) in adult F1 male mice. Sci Total Environ 728, 9. https://doi.org/10.1016/j.scitotenv.2020.138759.

[6] Del Moral, L.I., Le Corre, L., Poirier, H., Niot, I., Truntzer, T., Merlin, J.F., et al., 2016. Obesogen effects after perinatal exposure of 4,4 '-sulfonyldiphenol (Bisphenol S) in C57BL/6 mice. Toxicology 357 11–20. https://doi.org/10.1016/j.tox.2016.05.023.

[7] Meng, Z.Y., Wang, D.Z., Liu, W., Li, R.S., Yan, S., Jia, M., et al., 2019. Perinatal exposure to Bisphenol S (BPS) promotes obesity development by interfering with lipid and glucose metabolism in male mouse offspring. Environ Res 173, 189–198. https://doi.org/10.1016/j.envres.2019.03.038.

[8] Alexandre-Santos, B., Reis, G.D.S., Medeiros, G.R., Stockler-Pinto, M.B., Oliveira, N.S.C., Miranda-Alves, L., et al., 2024. Bisphenol S exposure induces cardiac remodeling and aggravates high-fat diet-induced cardiac hypertrophy in mice. Environ Res, 119781. https://doi.org/10.1016/j.envres.2024.119781.

[9] Brulport, A., Le Corre, L., Maquart, G., Barbet, V., Dastugue, A., Severin, I., et al., 2021. Multigenerational study of the obesogen effects of bisphenol S after a perinatal exposure in C57BL6/J mice fed a high fat diet. Environ Pollut 270, 11. https://doi.org/10.1016/j.envpol.2020.116243.

[10] Xiao, X., Zhang, X.W., Bai, J., Li, J., Zhang, C.Q., Zhao, Y.S., et al., 2021. Bisphenol S increases the obesogenic effects of a high-glucose diet through regulating lipid metabolism in Caenorhabditis elegans. Food Chem 339, 7. https://doi.org/10.1016/j.foodchem.2020.127813.

[11] Heindel, J.J., Skalla, L.A., Joubert, B.R., Dilworth, C.H., Gray, K.A., 2017. Review of developmental origins of health and disease publications in environmental epidemiology. Reprod Toxicol 68, 34–48. https://doi.org/10.1016/j.reprotox.2016.11.011.

[12] Deceuninck, Y., Bichon, E., Marchand, P., Boquien, C.Y., Legrand, A., Boscher, C., et al., 2015. Determination of bisphenol A and related substitutes/analogues in human breast milk using gas chromatography-tandem mass spectrometry. Anal Bioanal Chem 407 (9), 2485–2497. https://doi.org/10.1007/s00216-015-8469-9.

[13] Zhao, M., Xie, Y., Xu, X., Zhang, Z., Shen, C., Chen, X., et al., 2024. Reproductive and transgenerational toxicity of bisphenol S exposure in pregnant rats: insights into hormonal imbalance and steroid biosynthesis pathway disruption. Sci Total Environ 927, 172379. https://doi.org/10.1016/j.scitotenv.2024.172379.
[14] Ding, J., Ji, J., Rabow, Z., Shen, T., Folz, J., Brydges, C.R., et al., 2021. A metabolome atlas of the aging mouse brain. Nat Comm 12 (1). https://doi.org/10.1038/s41467-021-26310-y.
[15] Fasano, A., Chassaing, B., Haller, D., Ventura, E.F., Carmen-Collado, M., Pastor, N., et al., 2024. Microbiota during pregnancy and early life: role in maternal-neonatal outcomes based on human evidence. Gut Microbes 16 (1). https://doi.org/10.1080/19490976.2024.2392009.
[16] Maruvada, P., Leone, V., Kaplan, L.M., Chang, E.B., 2017. The human microbiome and obesity: moving beyond associations. Cell Host Microbe 22 (5), 589–599. https://doi.org/10.1016/j.chom.2017.10.005.
[17] Li, A., Zhuang, T., Shi, W., Liang, Y., Liao, C., Song, M., et al., 2020. Serum concentration of bisphenol analogues in pregnant women in China. Sci Total Environ 707, 136100. https://doi.org/10.1016/j.scitotenv.2019.136100.
[18] Ribeiro, E., Ladeira, C., Viegas, S., 2017. Occupational exposure to bisphenol A (BPA): a reality that still needs to be unveiled. Toxics 5 (3). https://doi.org/10.3390/toxics5030022.
[19] Schönfelder, G., Wittfoht, W., Hopp, H., Talsness, C.E., Paul, M., Chahoud, I., 2002. Parent bisphenol A accumulation in the human maternal-fetal-placental unit. Environ Health Perspect 110 (11), A703–707. https://doi.org/10.1289/ehp.110-1241091.
[20] Authority, E.F.S., 2007. Opinion of the Scientific Panel on food additives, flavourings, processing aids and materials in contact with food (AFC) related to 2,2-BIS(4-HYDROXYPHENYL)PROPANE. EFSA J 5 (1), 428. https://doi.org/10.2903/j.efsa.2007.428.
[21] Quan, L.H., Zhang, C.H., Dong, M., Jiang, J., Xu, H.D., Yan, C.L., et al., 2020. Myristoleic acid produced by enterococci reduces obesity through brown adipose tissue activation. Gut 69 (7), 1239–1247. https://doi.org/10.1136/gutjnl-2019-319114.
[22] Zeng, J., Yang, Z.Q., Zhong, Y., Zheng, Y.L., Hao, J.W., Luo, G., et al., 2022. Metabolomics insights into the interaction between Pseudomonas plecoglossicida and Epinephelus coioides. Sci Rep 12 (1). https://doi.org/10.1038/s41598-022-17387-6.
[23] Zhao, X.J., Zeng, Z.D., Chen, A.M., Lu, X., Zhao, C.X., Hu, C.X., et al., 2018. Comprehensive strategy to construct in-house database for accurate and batch identification of small molecular metabolites. Anal Chem 90 (12), 7635–7643. https://doi.org/10.1021/acs.analchem.8b01482.
[24] Wisniewski, J.R., Zougman, A., Nagaraj, N., Mann, M., 2009. Universal sample preparation method for proteome analysis. U360 Nat Methods 6 (5), 359. https://doi.org/10.1038/nmeth.1322.
[25] Wu, C., Lei, J., Meng, F., Wang, X., Wong, C.J., Peng, J., et al., 2023. Trace sample proteome quantification by data-dependent acquisition without dynamic exclusion. Anal Chem 95 (49), 17981–17987. https://doi.org/10.1021/acs.analchem.3c03357.
[26] Navarro, G., Allard, C., Xu, W.W., Mauvais-Jarvis, F., 2015. The role of androgens in metabolism, obesity, and diabetes in males and females. Obesity 23 (4), 713–719. https://doi.org/10.1002/oby.21033.
[27] Uchtmann, K.S., Taylor, J.A., Timms, B.G., Stahlhut, R.W., Ricke, E.A., Ellersieck, M.R., et al., 2020. Fetal bisphenol A and ethinylestradiol exposure alters male rat urogenital tract morphology at birth: confirmation of prior low-dose findings in CLARITY-BPA. Reprod Toxicol 91, 131–141. https://doi.org/10.1016/j.reprotox.2019.11.007.
[28] Reuter, S.E., Evans, A.M., 2012. Carnitine and acylcarnitines pharmacokinetic, pharmacological and clinical aspects. Clin Pharmacokinet 51 (9), 553–572.
[29] Petrus, P., Lecoutre, S., Dollet, L., Wiel, C., Sulen, A., Gao, H., et al., 2020. Glutamine Links obesity to inflammation in human white adipose tissue. Cell Metab 31 (2), 375. https://doi.org/10.1016/j.cmet.2019.11.019.
[30] Saito, M., Matsushita, M., Yoneshiro, T., Okamatsu-Ogura, Y., 2020. Brown Adipose tissue, diet-induced thermogenesis, and thermogenic food ingredients: from mice to men. Front Endocrinol 11. https://doi.org/10.3389/fendo.2020.00222.
[31] Prapaharan, B., Lea, M., Beaudry, J.L., 2024. Weighing in on the role of brown adipose tissue for treatment of obesity. J Pharm Pharm Sci 27, 13157. https://doi.org/10.3389/jpps.2024.13157.
[32] Lecoutre, S., Maqdasy, S., Rizo-Roca, D., Renzi, G., Vlassakev, I., Alaeddine, L.M., et al., 2024. Reduced adipocyte glutaminase activity promotes energy expenditure and metabolic health. Nat Metab 6 (7), 1329–1346. https://doi.org/10.1038/s42255-024-01083-y.
[33] Li, Z., Zhou, E.C., Liu, C., Wicks, H., Yildiz, S., Razack, F., et al., 2023. Dietary butyrate ameliorates metabolic health associated with selective proliferation of gut Lachnospiraceae bacterium 28-4. JCI Insight 8 (4). https://doi.org/10.1172/jci.insight.166655.
[34] Lai, K.K., Lorca, G.L., Gonzalez, C.F., 2009. Biochemical properties of two cinnamoyl esterases purified from a Lactobacillus johnsonii strain isolated from stool samples of diabetes-resistant rats. Appl Environ Microbiol 75 (15), 5018–5024. https://doi.org/10.1128/aem.02837-08.
[35] Andreasen, A.S., Larsen, N., Pedersen-Skovsgaard, T., Berg, R.M.G., Moller, K., Svendsen, K.D., et al., 2010. Effects of Lactobacillus acidophilus NCFM on insulin sensitivity and the systemic inflammatory response in human subjects. Br J Nutr 104 (12), 1831–1838. https://doi.org/10.1017/s0007114510002874.
[36] Wei, S.H., Chen, Y.P., Chen, M.J., 2015. Selecting probiotics with the abilities of enhancing GLP-1 to mitigate the progression of type 1 diabetes in vitro and in vivo. J Funct Foods 18, 473–486. https://doi.org/10.1016/j.jff.2015.08.016.
[37] Qiao, Y., Sun, J., Xia, S.F., Li, L.T., Li, Y., Wang, P.P., et al., 2015. Effects of different Lactobacillus reuteri on inflammatory and fat storage in high-fat diet-induced obesity mice model. J Funct Foods 14, 424–434. https://doi.org/10.1016/j.jff.2015.02.013.
[38] Petersen, C., Bell, R., Kiag, K.A., Lee, S.H., Soto, R., Ghazaryan, A., et al., 2019. T cell-mediated regulation of the microbiota protects against obesity. Science 365 (6451). https://doi.org/10.1126/science.aat9351.
[39] Sao Emani, C., Gallant, J.L., Wiid, I.J., Baker, B., 2019. The role of low molecular weight thiols in Mycobacterium tuberculosis. Tuberculosis 116, 44–55. https://doi.org/10.1016/j.tube.2019.04.003.
[40] Smith, E., Ottosson, F., Hellstrand, S., Ericson, U., Orho-Melander, M., Fernandez, C., et al., 2020. Ergothioneine is associated with reduced mortality and decreased risk of cardiovascular disease. Heart 106 (9), 691–697. https://doi.org/10.1136/heartjnl-2019-315485.
[41] Talmor-Barkan, Y., Bar, N., Shaul, A.A., Shahaf, N., Godneva, A., Bussi, Y., et al., 2022. Metabolomic and microbiome profiling reveals personalized risk factors for coronary artery disease. Nat Med 28 (2), 295. https://doi.org/10.1038/s41591-022-01686-6.